Received: 6 May 2024 | Revised: 19 August 2024 | Accepted: 26 August 2024

IET Power Electronics

DOI: 10.1049/pel2.12777

The Institution of Engineering and Technology WILEY

ORIGINAL RESEARCH

Time-domain design for misalignment-tolerant dynamic wireless charging

Juan Carlos Quirós | Álvaro Llamas Calvo | Alicia Triviño | Eliseo Villagrasa Guerrrero

Department of Electrical Engineering, Universidad de Malaga, Malaga, Spain

Correspondence
Juan Carlos Quirós, Department of Electrical Engineering, Universidad de Malaga, 29010 Malaga, Spain.
Email: quirosgil76@uma.es

Funding information
Junta de Andalucía, Grant/Award Number: PCM_00006

Abstract

Wireless power transfer (WPT) offers a safer and more convenient alternative to traditional charging methods. In the automotive sector, dynamic WPT presents a promising solution by reducing battery size and enhancing vehicle usability. The key components of dynamic WPT systems are the coils and their compensation topologies. This paper provides a detailed analysis of these elements to optimize system performance. First, different coil geometries are systematically evaluated using finite element analysis, aiming to identify designs that minimize electrical parameter variations, which can damage electronics and make the control more complex. Then, the most suitable compensation topology is determined through time-domain analysis, which is more accurate under dynamic conditions than the commonly used phasor-based approach. This design process based on time-domain analysis is validated with a 100 W dynamic charger prototype, demonstrating the system's transient behaviour. Experimental results show an efficiency of up to 80% and high tolerance to misalignment under various load conditions.

1 | INTRODUCTION

Over the last decades, governments have been moving towards a decarbonization process in order to reduce greenhouse effects and global warming. Since 1979 average and extreme temperatures as well as natural disasters have continuously increased and, far from stopping, they are expected to continue growing [1]. As a solution for these problems, electric vehicles (EVs) are set, as they help to reduce the amount of greenhouse effect gases in cities and they can also be combined with renewable energy sources [2].

The adoption of EVs faces relevant technological limitations. Their cost, autonomy and several safety issues in wired charging are some of the major problems making people reluctant to purchase this type of vehicle [3]. Charging based on wireless power transfer (WPT) has been proved to be an alternative for wired charging as it does not need a physical union between the energy source and the battery. Thus wireless charging is safer for the user. It also alleviates the problem concerning the autonomy as it can be implemented following several strategies like stationary charging and dynamic WPT (DWPT) [4].

There are several types of WPT technology depending on the distance and the method by which power is transmitted. Inductive power transfer (IPT) is set as the most mature of these technology due to its acceptable transferable distance and its high efficiency [4]. This technology uses magnetic fields to transmit power between a transmitter/primary and a receiver/secondary. In this scenario, DWPT can be implemented improving the autonomy of the vehicles and reducing the battery capacity needed. The generic diagram of DWPT is illustrated in Figure 1. However, DWPT charging must still address several technological challenges. As several coils are used to transmit power, the transferred power is not constant producing fluctuation in the batteries. Another problem in this kind of systems is that primary coils have to be turned on and off so that peaks appears producing component oversizing. In addition, these primary coils have coupling coefficient between them, which may lead to undesired and unexpected leakage fields. This can be solved by pulling apart coils, which make a more fluctuating output power with increased losses in the power converters [5]. In order to minimize these drawbacks, a precise design must be accomplished for the coupler and the compensation topology.

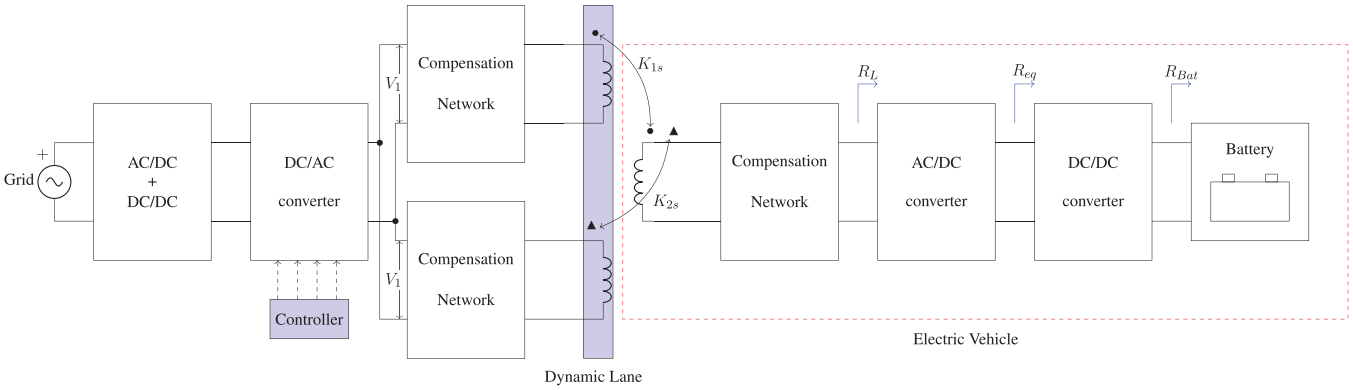

FIGURE 1 Generic DWPT charger scheme.

Several cities have implemented dynamic charging lanes to assess their feasibility. For instance, the OLEV project in South Korea [6], the Victoria project in Malaga (Spain) [7], the FastinCharge project in Douai (France) [8], and the Conductix-Wampfler project in Turin (Italy) [9] have all adopted this technology. Additionally, the Fabric project and the Smartroad Gotland project have conducted real-life trials of dynamic wireless charging. However, these research endeavours incur significant costs as they require the replication of coils and power electronics to enable uninterrupted dynamic charging along specific road sections. The information about how the coils were designed and the strategies followed in the power electronics control have not been detailed during the designing process or they are not public. This lack of information creates an unawareness in the optimization in the design process and in the control design. In addition to the electronics and coils, there is not relevant information about the compensation topologies used for these projects.

Alternatively, there are some research works that include some details about the design of the coils and the compensation systems. As for the coupler, the designs are mainly oriented to minimize fluctuation in the flux linkage to the secondary. Coupling designs focus on possible configuration, rail type couplers or multiple pad type in the primary side [10]. Rail type couplers achieve more constant coupling coefficient ($k_{i,s}$, where $i \epsilon \{N\}$ representing the number of primary coil in a N-coil lane and s refers to the secondary) although their level are lower than in multiple pad couplers. In multiple pad coupler design the goal is to achieve a constant power and $k_{i,s}$ on the secondary side. For this purpose several topologies have been proposed circular [11–15], rectangular/square [16–24], DD [25–31], DDQ [25, 28, 31], or bipolar [27, 30]. Other kind of geometries like I-type can be found in [32, 33]. These geometries are not that common as the previous ones and, consequently, there are not considered in our work.

Regarding the compensation topologies, their application for DWPT seeks to reduce the effects on the variation of the coupling and control. Thus, compensation systems are designed in order to achieve constant power on the secondary output. Series–series, LCC–LCC, and LCC–S are the most common topologies used in this kind of charger [11, 15, 16, 18–20, 23–26, 28–30, 32]. In these previous works, there is not an elaborated justification about how the geometries of the coils and the compensation systems are selected. Only the works in [20] compare different geometries of coils and in [11] different compensation topologies are discussed in order to find the most suitable option. Only studies in [22] do both comparisons. Both analysis were done in a sequential way, once the most suitable pair of coils are chosen in order to maximize coupling and quality factors of the topology designed. Although this study compares both, Compensation topology and coil geometry, the are some options that are not take into account, for example LCC–LCC or DD shape coils. Finally, in [34] a comparison between different coil geometries is done. Apart from this, an optimization algorithm is proposed in order to find the most suitable pair of coils. Table 1 summarizes the main features of the DWPT prototypes described in the related literature.

In this paper, we describe a sequential methodology in order to perform the final DWPT system. The work [35] proposes a design process in which the coupler and the compensation topology are both configured at the same time. This approach is also followed in [34]. However, with a sequential approach with two separate phases (for couplers and compensation topology), we can focus mostly on the critical part (the couplers) and then adjust the compensation system to them. First, we perform a comprehensive analysis of several coil designs to clearly justify the implementation of a DWPT system. Electrical parameters mainly guide this design step but there are other physical parameters to take into account such as coil dimensions, number of turns and amount of material needed. Once the geometry of the coil is defined, the most convenient compensation system is identified based on the principal electrical parameters of the coils, inductance, resistance, quality, and coupling factor. Although the design details are given for a proof-of-concept, we aim to set a systematic approach to be applied in other DWPT prototypes. The main features of the specific prototype considered in this paper are: air gap =190 mm, maximum width =340 mm and maximum length =400 mm. A bunch of experiments have also been performed in a 100 W prototype in laboratory. The validation of the simulations and analysis done in the

TABLE 1 Related work.

Paper	Analysis of coil geometry	Primary coil	Secondary coil	Analysis of compensation system	Compensation
[25]	×	DD	DDQ	×	LCC-LCC
[26]	×	DD	DD	×	LCC-LCC
[16]	×	Rectangular	Rectangular	×	LCC-LCC
[27]	×	DD	Bipolar	×	LCC-P
[17]	×	Rectangular	Rectangular	✓	T type-Series
[28]	×	DD/rectangular	DDQ	×	LCC–S
[11]	×	Circular	Circular	✓	LCC–S
[18]	×	Rectangular	Square	×	LCC-LCC
[19]	×	Rectangular	Rectangular	×	Series-Series
[12]	×	Rectangular	Circular	×	LCL-Series
[20]	✓	Rectangular	Rectangular	×	Series-Series
[21]	×	Rectangular	Rectangular	×	LCC-LCL
[22]	✓	Rectangular	Rectangular	✓	LCC-LCL
[29]	×	DD	Rectangular	×	LCC–S
[30]	×	DD	Bipolar	×	LCC-LCC
[13]	×	Circular	Circular	×	LSP-S
[31]	×	DD	DDQ	×	P-LC
[34]	✓	DD	DD	×	Series-Series
[32]	×	I-type	square	×	Series-Series
[24]	×	Rectangular	Rectangular	×	LCC-LCC
[33]	✓	I-type	Square	×	Series-Series
[15]	×	Circular	Circular	×	Series-Series
[23]	×	Square	Square	×	LCC-LCC
Proposal	✓	**Rectangular**	**Bipolar**	✓	**LCC-S**

paper have been tested in several situations, including efficiency in load variation and misalignment conditions. The magnetic design has also been tested by measuring the inductance values and comparing them with simulated results. Results shows an efficiency up to 80% and high tolerance to misalignment.

Thus, the main contributions of this work are:

- A coil design process where several geometries of coil are tested in order to find the most suitable coupler for this implementation. Specifically, we consider that a geometry of a coupler is a better option than another when it is less expensive while it provides a low variation of the mutual inductance in a wide range of misalignment. In this way, we cope with misalignment, which is inevitable in DWPT. With our approach, the negative effects associated to misalignment are minimized. Most papers in the literature review do not analyse different coil geometries for their implementation. They consider only one geometry [11–13, 15–19, 21–32], leading to limited analysis with a non-optimized design. In contrast to [17] where the author prioritize the compensation design, we prioritize the coil design as it is the most critical part of WPT systems. Thus, we have defined a first design stage to configure this element instead of a joint stage to determine the coils and the compensation topology at the same time.
- An analysis of different compensation topologies is performed in order to find the perfect solution for this charger. In order to achieve more precise results, a time domain analysis is performed. Most papers in the related work only analyze the equivalent circuits with a first harmonic approximation (FHA), which leads to imprecise results. FHA method does not solve discrete stationary problems without considering transient stages or previous values of voltage and current in capacitors and coils. In this work, we use time domain analysis in order to compare the compensation topologies. In this way, more harmonics are considered in a superposition approach, giving a more precise result.
- We have conducted a set of experimental analyses on a prototype vehicle in order to validate the coil design and characterize voltage, current, efficiency and dynamic behaviour of the proposed DWPT system. The results confirm the accuracy of our theoretical analysis.

The paper is organized as follows. In Section 2 the magnetic design of the primary and secondary coil and the optimization process for the primary coil are done. In Section 3, a comparative between the main compensation topologies is performed based on a time domain analysis. In Section 4 the set of experiments conducted on the prototype as well as their result are shown. Finally, in Section 5 several conclusions drawn from this papers work can be found.

2 | COUPLER DESIGN

In this section different coil pads configurations will be analysed in order to find the most suitable coupler for the DWPT prototype. The main objective of this analysis is finding the pair of coils that minimizes the cost of production of a lane while maintaining the coupling factor high and as constant as possible. To carry out this analysis the design process and calculations are done by the finite element analysis (FEA) tool ANSYS Maxwell. With this software the values of mutual inductance are obtained for several positions during the movement process as done in [36] and [37]. For every position the eddy currents effects have been considered. With the obtained data, a continuous equation for mutual inductance depending on displacement is developed. This equation is obtained through a polynomial regression which will be lately used for the time domain analysis. As the considered speed for the experiments is much lower than the operating frequency of the WPT system, it will not be considered. Anyway, the speed of the vehicle is relevant to know the energy acquired in the wireless power transfer. Higher the speed, less energy received in the battery due to the reduced charging time. The speed has also a relevant impact on the control as it affects the robustness of the control algorithm. For high speed, a control strategy capable of adapting quickly to the variations in coupling coefficients is needed.

In our experiments, we can conclude that the output power profile when charging the battery is mainly influenced by factors such as coil size, geometry and layout. The speed has a relevant impact on the output power profile when the vehicle is traversing several primary coils and the power transfer has to be transferred from one primary coil to another. A smaller distance between the primary coils results in a power profile with shorter periods of no energy due to the switching of the primary coils. However, it also amplifies the interaction between the primary coils, making it a complex issue to deal with in the control algorithm. Larger primary coils even more separated contribute to a more stable power profile but they also reduce the coupling coefficient. We focus on the design of the primary and the secondary coils without analysing the distance between the primary coils, as it is out of the scope of this work. Several topologies will be considered for the primary and secondary sides. All the simulations and analysis bellow will be done considering an operating frequency (f) of 85 kHz. The incorporation of ferrite tiles will not be considered for this study as it adds more complexity to the analysis (identification of the best arrangements of the ferrite tiles and more time-consuming simulations). Anyway, some preliminary works [38] shows that the shape of the profile of the coupling coefficient is not affected. The main variation when including the ferromagnetic material is the vertical displacement of the curve due to an increment in the coupling coefficient.

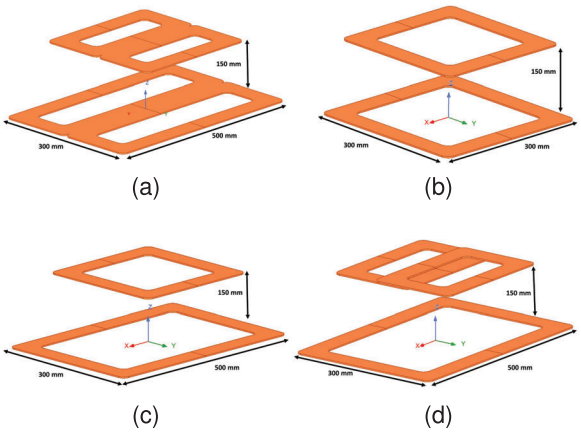

FIGURE 2 Analysed coil geometries. (a) DD–DD. (b) Square–square. (c) Rectangular—square. (d) Rectangular–bipolar.

One of the major requirements in this paper is achieving a low cost prototype, for this reason ferrite will not be considered in the analysis. Figure 2 show $k_{i,s}$ for the tested combinations of coils. These configuration are: square–square, rectangular–square, DD–DD and rectangular–bipolar. These topologies have been selected as they are widely used in the related work as summarized in Table 1.

The magnetic field of these geometries is altered differently when there is coil misalignment, as illustrated in Figure 3.

In order to choose the best option for this solution we will attend to the capability of achieving the higher coupling factor between coils and maintaining it as constant as possible throughout the displacement of the secondary coil. For this analysis, we consider the specific features where the DWPT will be installed (960 mm length and 300 mm width according to the prototype considered in this work).

Figure 4 shows the effect of misalignment in the X-axis direction (displacement direction) on the coupling factor for the analysed geometries. This analysis has been done considering the same coil sizes condition of sizes in order to have a realistic comparison, that is, 15 turns 350 × 500 mm^2 for the primary coil and 15 turns 300 × 300 mm^2 for the secondary coil. Although it can be seen that the most constant coupling factor occurs for the DD–DD geometry, its average value is poor when compared to the other three geometries. The square–square geometry achieves the highest coupling factor but it cannot be maintained constant throughout the entire range of misalignment. Regarding rectangular–square geometry, its behaviour is an intermediate option between the two previous geometries. Finally, rectangular–bipolar geometry achieves a high coupling factor while being able to maintain it constant for a wide range of misalignment. Thus, this last geometry is considered the most suitable one and will be used in the rest of the design process. This analysis has been considered with cost-effective coils in which no ferrite tiles have been incorporated. It is expected that the use of ferromagnetic materials

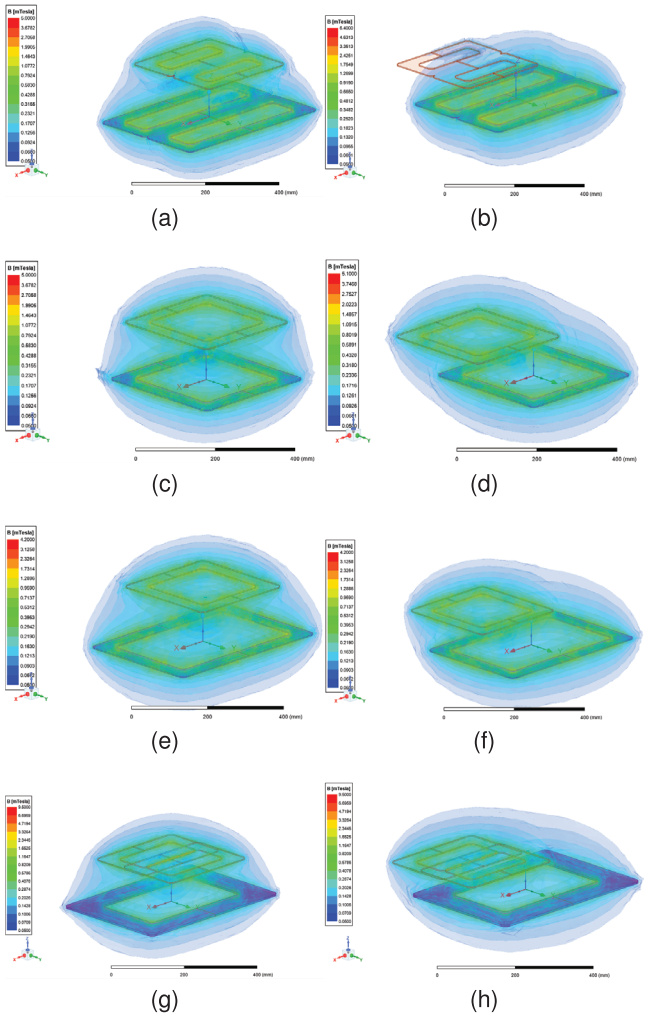

FIGURE 3 Magnetic field distribution. (a) 0-mm misalignment for DD-DD geometry. b) 200-mm misalignment for DD–DD geometry. (c) 0-mm misalignment for square–square geometry. d) 200-mm misalignment for square–square geometry. e) 0-mm misalignment for rectangular–square geometry. f) 200-mm misalignment for rectangular–square geometry. g) 0-mm misalignment for rectangular–bipolar geometry. h) 200-mm misalignment for rectangular–bipolar geometry.

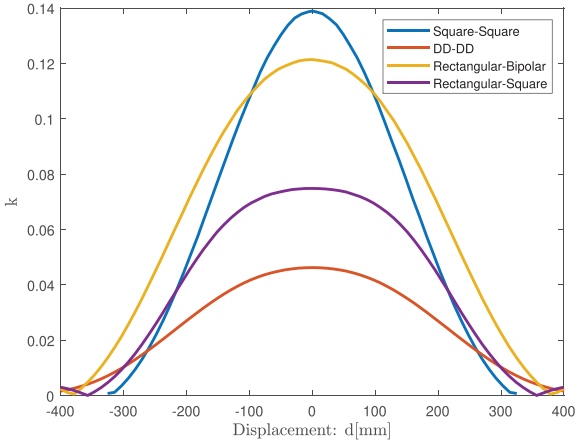

FIGURE 4 Coupling factor of the analysed geometries for misalignment in the *X*-axis direction.

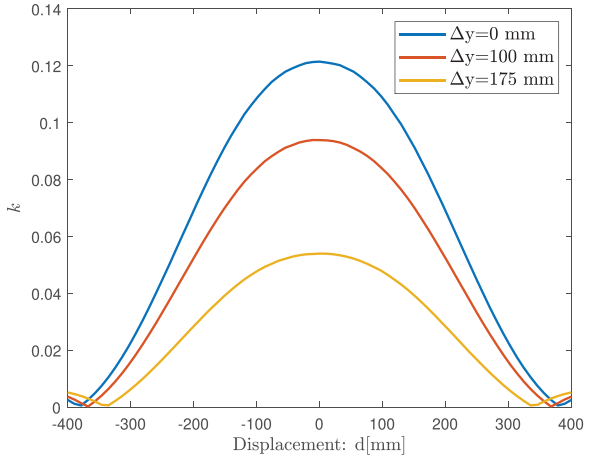

FIGURE 5 Tolerance of bipolar pad to lateral misalignment.

would change these profiles by raising the coupling but not the shape of the coupling profile.

Another convenient feature of the chosen topology is its tolerance to lateral misalignment (*Y*-axis misalignment). In Figure 5 the coupling factor for 0, 100, and 175 mm lateral misalignment is shown for the most suitable geometry that is the rectangular–bipolar pad. It can be seen that it can maintain the coupling factor at high levels and thus it can keep an efficient wireless power transfer. Considering a 300 mm coil width, the coupling coefficient decreases to the 75% of its maximum value for a 33% of *Y*-axis misalignment. For a 58% of *Y*-axis misalignment, k decrease to a 41.6% of its maximum value. The decrease is no linear, for the decrease of k is bigger for higher misalignments.

Next step in the design process is optimizing both coils. Due to the high air gap and the constructive constraints of the prototype the secondary coil will be fixed at its maximum achievable size. Thus, the bipolar pad outer dimensions are 300×300 mm^2 with 15 turns of 5 mm diameter AWG 38 Litz wire per coil. In bipolar pads it is crucial to find the optimal width of the coils in order to achieve zero coupling factor between them. This prevents both coils from inducing each other resulting in power losses on the secondary side. Figure 6 shows that the width of the coils that causes the zero coupling factor between them is 196 mm.

For the primary coil, the number of turns and diameter of the wire are the same as for the secondary coil in order to find symmetry between inductance values. The parameters to change in order to find the optimized size is the geometrical dimensions of the coils. Regarding the length, its dimension must be large enough to guarantee a high and constant coupling factor but small enough not to exceed the length of the vehicle. Thus, the length of the primary coil has been fixed at 500 mm, which not exceed the maximum length. According to this previous consideration the only geometrical dimension left that can be optimized is the coil width. Figure 7 represents the coupling factor for perfectly aligned coils as a function of the primary coil width. As shown in the graphic the optimal width is in between

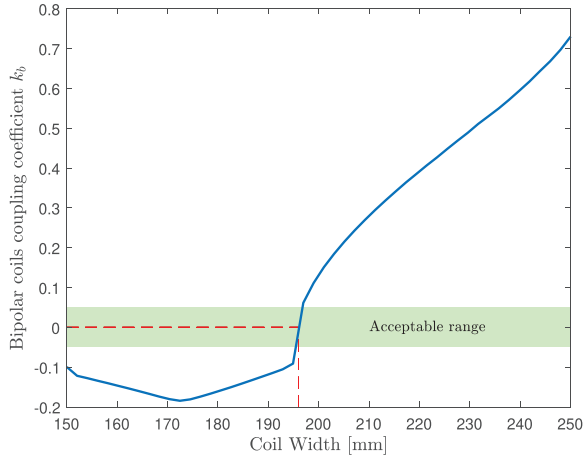

FIGURE 6 Coupling factor between coils composing the bipolar pad.

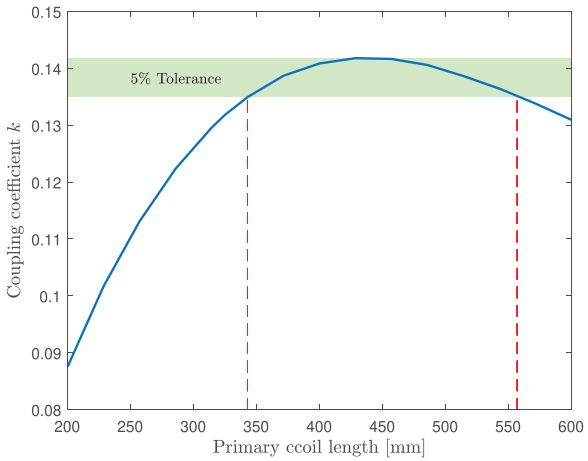

FIGURE 7 Primary coil length optimization.

400 and 450 mm but there is a wide range of high coupling factor ($k_{i,s} > 0.12$) for width between 340 and 560 mm. Due to geometrical restrictions of the prototype the width of the coil cannot be larger than the distance between wheels and then the width of the primary coil will be fixed at 320 mm allowing the displacement of the prototype over the coils as shown in Figure 10.

3 | COMPENSATION TOPOLOGY

Once the geometry of the coil is decided, it is necessary to judiciously determine the compensation system because the electrical parameters are greatly impacted by these structures. In particular, we analyse series–series, LCC–LCC and LCC–S, as they are the most representative compensation topologies in the literature related to DWPT. Their suitability will be evaluated according to the peak values of the primary and secondary currents. Excessive peaks could stress and even deteriorate the power converters, leading to a poor performance of the whole system in a short time. The compensation topology also

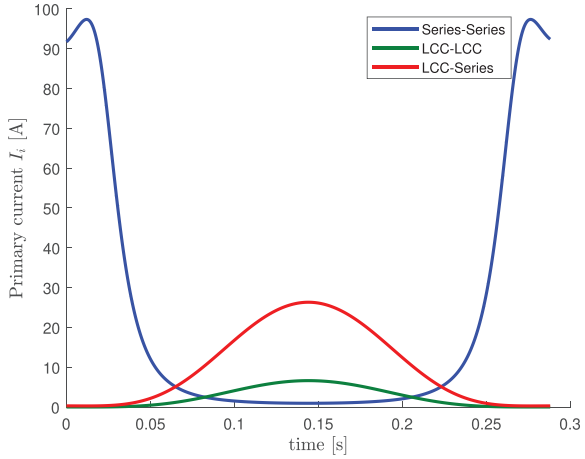

FIGURE 8 Primary current for different compensation topologies.

determine the behaviour of the output, which can be constant voltage (CV) or constant current (CC) [10]. In addition, a precise design of these compensation system will determine the behaviour of the efficiency under changes in coupling, intrinsically present in DWPT. Since the coupling coefficient varies when the secondary coil traverses the primary coil, we consider that a time-domain analysis is more accurate than a phasor-based study. In contrast to [11], we base the design of the compensation topology in the time-domain analysis to study the transient effects, which are omitted in the phasor-based analysis. Table 2 shows the time domain analysis mesh equations for the different compensation topologies considered in this paper. It also shows the AC–AC (from inverter output to rectifier input) equation for the proposed topologies. In order to achieve a precise excitation for the analytical process, the Fourier transform of a square signal is used. This Fourier approximation considers the first 9 harmonics. With this excitation we can obtain a close approximation to the inverter output voltage and thus, predict the performance of the system.

In order to select the right components, a mathematical model is necessary. This model must determine the values of current and voltages accurately. Most Papers make this analysis using a model based on phasors, as a concatenation of static solutions. With such approach, transient analysis is omitted, which may derive in relevant conditions that must be considered in the design. Accordingly, we have proceeded with a time-domain analysis which includes the transient period. To simplify the model, an equivalent load resistance (R_L) is defined. The value of R_L depends on D, where D represents the duty cycle of the secondary side DC/DC converter (boost type for this analysis), R_{Bat} represent the equivalent resistance of the battery and R_{eq} represents the battery equivalent resistance before the boost converter.

$$R_{eq} = (1 - D)^2 R_{Bat} \tag{4}$$

$$R_L = \frac{8}{\pi^2} R_{eq} \tag{5}$$

Figures 8 and 9 show the RMS currents on the primary and secondary sides respectively for the same power transfer

TABLE 2 Mesh equations in a time-domain analysis for the proposed compensation topologies.

Topologies	Schematics	Electrical analysis
Series–series	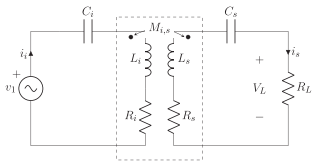	$$\frac{dv_1(t)}{dt} = \frac{1}{C_i} i_i(t) + R_i \frac{di_i(t)}{dt} + L_i \frac{d^2 i_i(t)}{dt^2} - M_{i,s}(t) \frac{d^2 i_s(t)}{dt^2}$$ $$0 = -(R_L + R_s) \frac{di_s(t)}{dt} - \frac{1}{C_s} i_s(t) - L_s \frac{d^2 i_s(t)}{dt^2} + M_{i,s}(t) \frac{d^2 i_{p,i}(t)}{dt^2}$$ $$\eta_{SS}{}^{AC} = \frac{R_L}{(R_L + R_2) + \left(1 + R_1 \frac{(R_2 + R_L)}{w^2 M_{i,s}(t)^2}\right)} \quad (1)$$
LCC–series	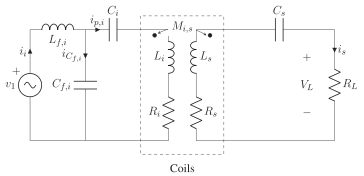	$$\frac{dv_1(t)}{dt} = L_f \frac{d^2 i_i(t)}{dt^2} + \frac{1}{C_{f,i}} i_i(t) - \frac{1}{C_{f,i}} i_{p,i}(t)$$ $$0 = -\frac{1}{C_{f,i}} i_i(t) + \frac{1}{C_{f,i}} i_{p,i}(t) + \frac{1}{C_i} i_{p,i}(t) + R_i \frac{di_{p,i}(t)}{dt} + L_i \frac{d^2 i_{p,i}(t)}{dt^2} - M_{i,s}(t) \frac{d^2 i_s(t)}{dt^2}$$ $$0 = -(R_L + R_s) \frac{di_s(t)}{dt} - \frac{1}{C_s} i_s(t) - L_s \frac{d^2 i_s(t)}{dt^2} + M_{i,s}(t) \frac{d^2 i_{p,i}(t)}{dt^2}$$ $$\eta_{LCC\text{–}S}{}^{AC} = \frac{(w^2 L_{f,i} M_{i,s}(t))^2 R_L}{\frac{(wL_{f,i})^2 (R_s + R_L)}{R_i (R_s + R_L) + (wM_{i,s}(t))^2} (R_s + R_L)^2 \left(R_i + \frac{(wM_{i,s}(t))^2}{R_s + R_L}\right)^2} \quad (2)$$
LCC–LCC	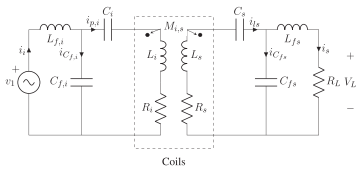	$$\frac{dv_1(t)}{dt} = L_{f,i} \frac{d^2 i_i(t)}{dt^2} + \frac{1}{C_{f,i}} i_i(t) - \frac{1}{C_{f,i}} i_{p,i}(t)$$ $$0 = -\frac{1}{C_{f,i}} i_i(t) + \frac{1}{C_{f,i}} i_{p,i}(t) + \frac{1}{C_i} i_{p,i}(t) + R_i \frac{di_{p,i}(t)}{dt} + L_i \frac{d^2 i_{p,i}(t)}{dt^2} - M_{i,s}(t) \frac{d^2 i_{ls}(t)}{dt^2}$$ $$0 = -\frac{1}{C_{fs}} i_s(t) + \frac{1}{C_{fs}} i_{ls}(t) + \frac{1}{C_s} i_{ls}(t) + R_s \frac{di_{ls}(t)}{dt} + L_s \frac{d^2 i_{ls}(t)}{dt^2} - M_{i,s}(t) \frac{d^2 i_{p,i}(t)}{dt^2}$$ $$0 = L_{fs} \frac{d^2 i_s(t)}{dt^2} + \frac{1}{C_{fs}} i_s(t) - \frac{1}{C_{fs}} i_{ls}(t) + R_L \frac{di_s(t)}{dt}$$ $$\eta_{LCC}{}^{AC} = \frac{M_{i,s}(t)^2 \omega^4 R_L L_{fs}^2}{R_i \omega^4 L_{fs}^2 + (2R_i R_s R_L \omega^2 + M_{i,s}(t)^2 \omega^4 R_L) L_{fs}^2 + R_i R_s^2 R_L^2 + \omega^2 M_{i,s}(t)^2 R_s R_L^2} \quad (3)$$

conditions, that is, 100-W power transfer at 10 m/s with the coupler designed in the previous stage. It can be seen that LCC–LCC and LCC–S have a similar behaviour under misalignment conditions with a variation of $M_{i,s}(t)$. Series–series compensation has the disadvantage of increasing the current with low values of $M_{i,s}$. This behaviour is produced due to the low values of impedance reflected on the primary side. This characteristic makes the system achieve high values of current and thus making this topology inappropriate for DWPT systems. On the other hand, LCC–LCC and LCC–S rise the current values for higher values of $M_{i,s}$. This characteristic makes these topologies a suitable option due to the fact that higher values of current do not appear when there is no secondary coil, event with a high probability in DWPT systems. For low values of $M_{i,s}$ the current maintain its value in a constant level. The relation between the output power and the primary current depends directly on the inductance filter values of the compensation. According to [39], the values of the filter are selected to increase the efficiency maintaining low values of input current. This filter value has to be carefully chosen because high values also produce a rise of harmonic distortion.

From the previous results, the LCC–S compensation will be chosen because it has an acceptable variation of the primary current and a similar performance of the secondary current when compared to the LCC–LCC structure. Moreover, LCC–S needs less components, which reduces the cost and weight of the DWPT system. The series capacitor of the secondary topology also gives a CV behaviour which can be interesting in this kind of charger.

Finally the expression that defines the efficiency of the system can be found in Table 2 for the three analysed compensation topologies. The expression of the efficiency takes into account

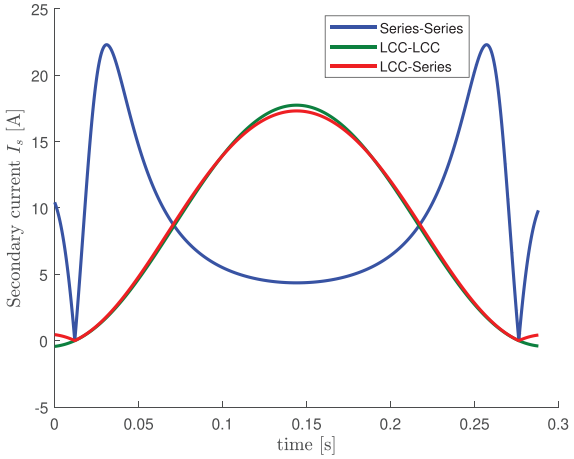

FIGURE 9 Secondary current for different compensation topologies.

TABLE 3 AC–AC efficiency comparative.

Coil geometry	Peak efficiency	Efficiency 50%
DD–DD	78.2%	55.96%
Square–square	93.36%	66.40%
Rectangular–square	92.13%	78.27%
Rectangular–bipolar	**93.76%**	**85.44%**

the losses due to the coil resistances. It can be seen that the efficiency depends on the load resistance value, the filter coil value ($L_{f,i}$) and the coupling coefficient given by $M_{i,s}$.

To reaffirm the coil design, we have conducted a comparative study of the system efficiency for the coil geometries analysed in the previous section when LCC–series compensation is installed in the charger. In this analysis the peak efficiency value and the efficiency at a 50% of misalignment are compared under the same conditions. The efficiency has been measured comparing the output power of the primary inverter with the input power of the secondary rectifier. As the coupling changes, the efficiency also varies. Thus, we have measured the efficiency in two conditions: with the coils perfectly aligned (peak efficiency) and when the secondary coil has 50% displacement ($\text{Efficiency}_{50\%}$). In Table 3, the main results are summarized. It can be observed that the coil geometry selected previously still outperforms the others when LCC–series is used. Specifically, it is notable the reduced variation of the efficiency for misalignment conditions.

In real implementations, the wireless charger may incorporate some shielding structures to prevent the magnetic field to escape from the area of interest. Under these circumstances, the electrical model of the coupler changes, as verified in [40]. Since the chassis or other metallic structures have higher dimensions than the coils, we state that the variation of the electrical model is constant for all the misalignment conditions. This implies that the self-inductances and the mutual inductances are decremented by the same corresponding quantity for the whole range of misalignment conditions. Similarly, the equivalent resistances should experience a constant increment in the moving range. Consequently, we consider that the inclusion of these structures would lead to similar conclusions as the ones derived in our work.

4 | EXPERIMENTAL VALIDATIONS

In this section a series of experimental tests are conducted in order to validate the design process. Specifically, the design is applied to a HOMCOM 370-142V90u car, which is illustrated in Figure 10. The inverter is made with a KIT8020-CRD-8FF1217P-1 formed by SiC MOSFETs and the rectifier with Schottky diodes. The activation pulses for the inverter are controlled by a STM32. In this implementation, two primary coils have been installed in order to create a lane for DWPT charging. They have a distance between them to prevent interactions between primary coils. Each coil is fed by its own inverter and compensation network. These inverters are constantly working so that the transmitter coils are always powered. As the power consumption is low the losses when there is no receiver are negligible. The main aim of this decision is that there is no need of complex control system to detect the receiver coil position, which is out of the scope of this paper. The coils used for these experiments are shown in Figure 11 and their electrical parameters, which have been measured with a LCR HM812 meter, are summarized in Table 4. Due to the low power in the system, the magnetic fields will not be considered in this paper due to its negligible level. The levels of the magnetic field involved in this application do not represent any danger or interferences to the equipment. Consequently, the measurements in this section will consider only electrical parameters.

Figure 12 shows voltage ($v_1(t)$) and current ($i_1(t)$) on the primary side for the entire range of movement whereas Figure 13 shows voltage and current in the primary and secondary circuits respectively for the perfect alignment condition. First, we observe that the voltage is not a sine wave, which validates the need for other types of analysis not restricted to one phasor. It can be seen that when the secondary coil moves along the primary coil, current increases as the coupling factor does. On the opposite side, when the secondary coil is no longer coupled with

FIGURE 10 Implemented prototype for DWPT.

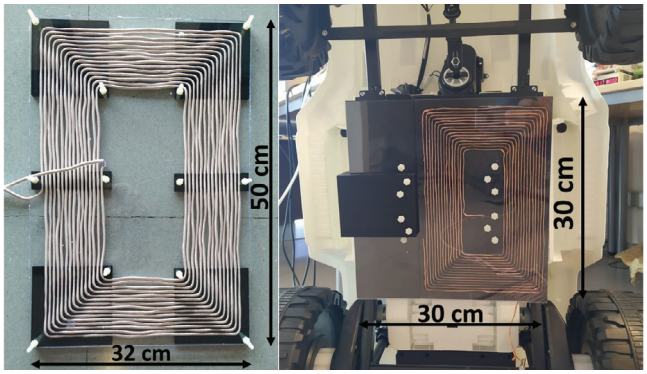

FIGURE 11 Implemented coils. (a) Primary rectangular pad. (b) Secondary bipolar pad.

TABLE 4 Electrical parameters of the implemented coils.

Parameter	Value
L_1 (μH)	112.18
L_s (μH)	110.92
R_1 (mΩ)	203.37
R_s (mΩ)	643.50
$L_{f,1}$ (μH)	40
$C_{f,1}$ (nF)	89.6
C_1 (nF)	52.3
C_s (nF)	31.8
f (kHz)	85

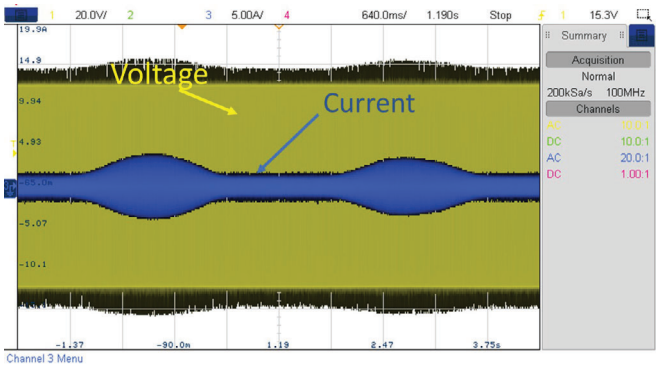

FIGURE 12 Voltage and current on a DWPT charging system with a two-coil lane.

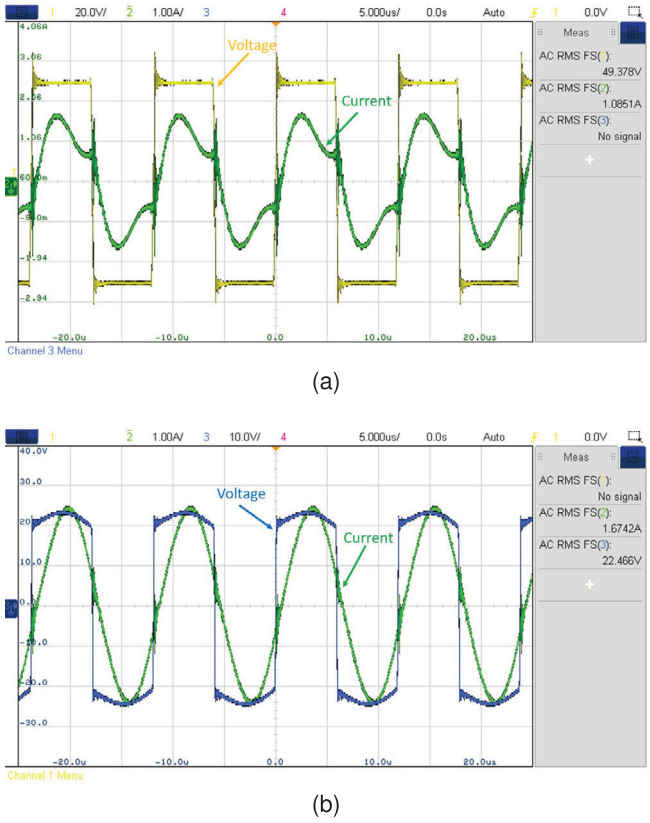

FIGURE 13 Voltage and current in the implemented prototype with aligned coils. (a) Primary side. (b) Secondary side.

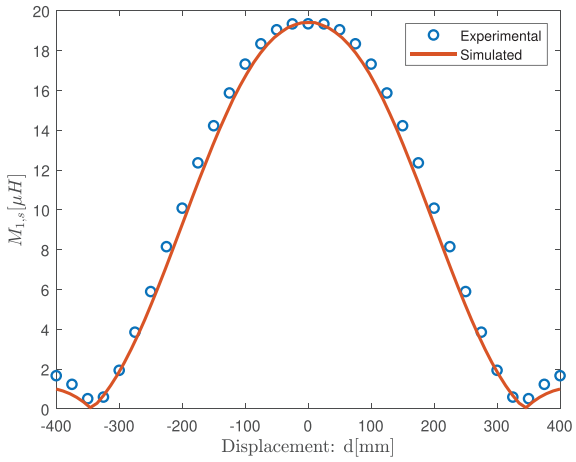

FIGURE 14 Simulated and measured mutual inductance throughout displacement.

the primary coil current decreases to a constant value. It can also be observed that there is no significant transient in current when the secondary coil switches from one primary coil to the next one due to the advantages provided by the compensation systems selected and the coil geometry.

Figure 14 shows the experimental and simulated values of mutual inductance between primary and secondary coils. The mutual inductance has been measured with a LCR meter HM812. It can be seen that, as expected, the graphic is symmetrical and the maximum values are achieved in the perfect alignment conditions. In addition, experimental and simulated results are significantly close to each other validating our proposed design. The small difference between these results can be produced by the LCR meter's measurement accuracy.

In order to determine whether the load affects the systems performance or not, several experiments for different loads have been conducted. It is worth noting that the equivalent

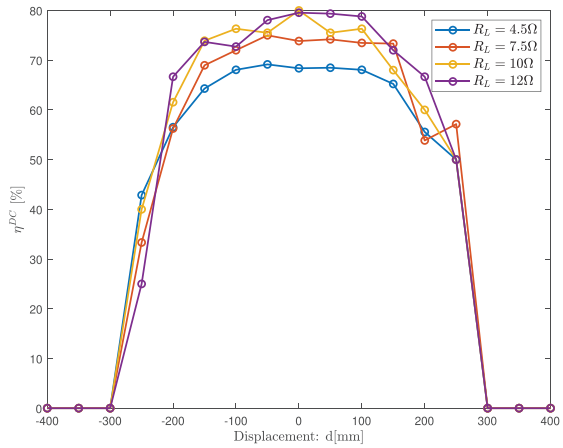

FIGURE 15 Measured DC–DC efficiency for different loads.

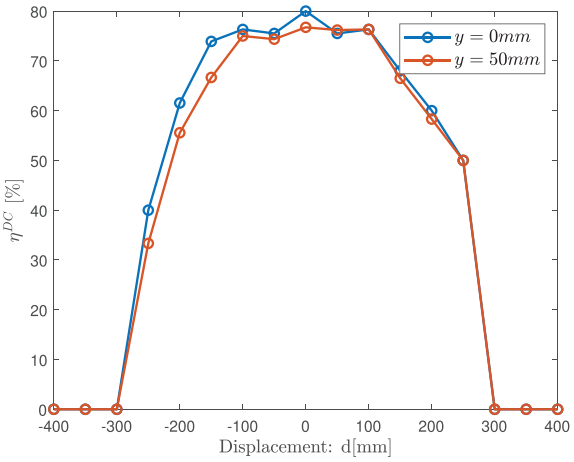

FIGURE 16 Measured DC–DC efficiency for 0 and 50 mm lateral misalignment.

resistance of the battery changes during its charging process. A range between 4.5 and 12 Ω has been chosen in order to recreate a resistance variation with the state of charge of the battery. 4.5 Ω would represent the maximum charging power situation and the rise of R_{Bat} represents the decreasing charging power. As soon as the charging power decreases and SoC rises, the equivalent resistance of the battery increases. Figure 15 shows the DC–DC efficiency (η^{DC}) of the system for different loads while the car is moving. This efficiency has been measured taking data from the power source (input of the primary side inverter) and the electronic load (working as a battery) throughout the movement process. This data has been taken every 5 cm.. The efficiency (η^{DC}) is defined as the efficiency between the AC/DC primary converter and the battery (see Figure 1). It can be seen that the maximum values of efficiency are achieved between values ranging 10 to 12 Ω while lower load values, like 4.5 Ω, imply lower efficiencies.

Finally, in the last experiment the performance of the system under lateral misalignment is analysed. For this experiment a 10 Ω load is selected and the efficiency η^{DC} for 0 and 50 mm lateral misalignment is measured and compared. Figure 16 shows the experimental results obtained in the laboratory. It can be seen that the effect of a lateral misalignment of 50 mm is almost negligible when compared to non-lateral misalignment. Thus, it can be concluded that the proposed system has an adequate performance under lateral misalignment, which is an important feature in DWPT systems.

5 | CONCLUSIONS

In WPT and DWPT systems, a thorough analysis of coil geometries is essential to determine the most suitable design for specific operating conditions. Our analysis concludes that the rectangular-bipolar geometry is the most effective for the proposed DWPT system. We have not considered the inclusion of ferrites. While the incorporation of this material would reduce coil size and improve performance, its complex integration was beyond the scope of this study.

The configuration of rectangular–bipolar coils requires the careful determination of the coil width in order to avoid overlap and ensure a zero coupling factor between coils. Optimizing the primary coil width also reveals a broad range of values that maintain a high coupling factor, allowing flexibility in design without significantly affecting performance under no misalignment. However, lateral misalignment tolerance decreases as coil width narrows.

Regarding the compensation network, the LCC–S topology is well-suited for DWPT systems, as it reduces primary current when the coupling factor decreases, enabling a standby mode that simplifies the control when there are switching of coils along an electrified lane. The absence of current transients during coil transitions further supports this conclusion. Overall, the proposed design and its implementation through a prototype vehicle validate the feasibility of an LCC–S compensated DWPT system.

Finally, our experiments demonstrate the existence of an optimal load for the secondary circuit, crucial for maximizing system efficiency. This optimal load can be maintained under varying battery conditions by using a DC–DC converter between the rectifier and the actual load. Future research will focus on developing control strategies to enhance overall system efficiency and manage power coil activation as the vehicle moves along the dynamic lane. We will also explore the use of ferromagnetic materials to further increase coupling efficiency.

AUTHOR CONTRIBUTIONS

Juan Carlos Quirós: Conceptualization; investigation; methodology; validation; writing—original draft; writing—review and editing. **Álvaro Llamas Calvo**: Investigation; methodology; validation. **Alicia Triviño**: Funding acquisition; supervision; validation; writing—review and editing. **Eliseo Villagrasa Guerrero**: Resources; writing—review and editing.

ACKNOWLEDGEMENTS

This work was supported in part by Universidad de Málaga and Junta de Andalucía under de project "PCM_00006".

CONFLICT OF INTEREST STATEMENT

The authors declare no conflicts of interest.

DATA AVAILABILITY STATEMENT

Research data are not shared.

ORCID

Juan Carlos Quirós https://orcid.org/0000-0002-4604-3028
Alicia Triviño https://orcid.org/0000-0002-7516-2878

REFERENCES

1. Breckner, M., Sunde, U.: Temperature extremes, global warming, and armed conflict: new insights from high resolution data. World Dev. 123, 104624 (2019)
2. Sharifi, P., Banerjee, A., Feizollahi, M.J.: Leveraging owners flexibility in smart charge/discharge scheduling of electric vehicles to support renewable energy integration. Comput. Ind. Eng. 149, 106762 (2020)
3. Statharas, S., Moysoglou, Y., Siskos, P., Zazias, G., Capros, P.: Factors influencing electric vehicle penetration in the EU by 2030: a model-based policy assessment. Energies 12(14), 2739 (2019)
4. Triviño, A., González González, J.M., Aguado, J.A.: Wireless power transfer technologies applied to electric vehicles: a review. Energies 14(6), 1547 (2021)
5. González González, J.M., Triviño Cabrera, A., Aguado, J.A.: Assessment of the power losses in a SAE J2954-compliant wireless charger. IEEE Access 10, 54474–54483 (2022)
6. Foote, A., Onar, O.C.: A review of high-power wireless power transfer. In: 2017 IEEE Transportation Electrification Conference and Expo (ITEC), pp. 234–240. IEEE, Piscataway, NJ (2017)
7. Victoria project | wireless charging system invehicles. https://www.fcirce.es/en/smart-mobility-en-en/victoria-2. Accessed 9 March 2024
8. Innovative fast inductive charging solution for electric vehicles | fastincharge | project | news & multimedia | fp7 | cordis | european commission. https://cordis.europa.eu/project/id/314284/reporting/es. Accessed 22 Feb 2024
9. Wireless charging for quiet and clean public transport in Torino (Italy) | eltis. https://www.eltis.org/discover/case-studies/wireless-charging-quiet-and-clean-public-transport-torino-italy. Accessed 1 Dec 2023
10. Bagchi, A.C., Kamineni, A., Zane, R.A., Carlson, R.: Review and comparative analysis of topologies and control methods in dynamic wireless charging of electric vehicles. IEEE J. Emerging Sel. Top. Power Electron. 9(4), 4947–4962 (2021)
11. Feng, H., Cai, T., Duan, S., Zhao, J., Zhang, X., Chen, C.: An LCC-compensated resonant converter optimized for robust reaction to large coupling variation in dynamic wireless power transfer. IEEE Trans. Ind. Electron. 63(10), 6591–6601 (2016)
12. Dai, X., Jiang, J.C., Wu, J.Q.: Charging area determining and power enhancement method for multiexcitation unit configuration of wirelessly dynamic charging EV system. IEEE Trans. Ind. Electron. 66(5), 4086–4096 (2019)
13. de Freitas Lima, G., Godoy, R.B.: Modeling and prototype of a dynamic wireless charging system using LSPS compensation topology. IEEE Trans. Ind. Appl. 55(1), 786–793 (2019)
14. Quirós, J.C., Guerrero, E.V., Sangeno, J.K., Triviño, A.: Magnetic integration of circular pads and LCC-LCC for EV wireless charging tolerant to misalignment. IEEE Access 11, 98558–98565 (2023)
15. Chen, K., Ouyang, Y., Yang, X., Cheung, N.C., Cheng, E.K.W., Pan, J.: A high-interoperability optimal frequency control method for the AGV dynamic wireless charging systems without communication. IEEE Trans. Power Electron. 39(3), 3797–3808 (2024)
16. Lu, F., Zhang, H., Hofmann, H., Mi, C.C.: A dynamic charging system with reduced output power pulsation for electric vehicles. IEEE Trans. Ind. Electron. 63(10), 6580–6590 (2016)
17. Zhao, J., Cai, T., Duan, S., Feng, H., Chen, C., Zhang, X.: A general design method of primary compensation network for dynamic WPT system maintaining stable transmission power. IEEE Trans. Power Electron. 31(12), 8343–8358 (2016)
18. Zhu, Q., Wang, L., Guo, Y., Liao, C., Li, F.: Applying LCC compensation network to dynamic wireless EV charging system. IEEE Trans. Ind. Electron. 63(10), 6557–6567 (2016)
19. Jeong, S.Y., Park, J.H., Hong, G.P., Rim, C.T.: Autotuning control system by variation of self-inductance for dynamic wireless EV charging with small air gap. IEEE Trans. Power Electron. 34(6), 5165–5174 (2019)
20. Zhang, Z., Pang, H., Lee, C.H.T., Xu, X., Wei, X., Wang, J.: Comparative analysis and optimization of dynamic charging coils for roadway-powered electric vehicles. IEEE Trans. Magn. 53(11), 1–6 (2017)
21. Tavakoli, R., Dede, E.M., Chou, C., Pantic, Z.: Cost-efficiency optimization of ground assemblies for dynamic wireless charging of electric vehicles. IEEE Trans. Transp. Electrif. 8(1), 734–751 (2022)
22. Cai, C., Wang, J., Fang, Z., Zhang, P., Hu, M., Zhang, J., et al.: Design and optimization of load-independent magnetic resonant wireless charging system for electric vehicles. IEEE Access 6, 17264–17274 (2018)
23. Li, H., Tan, L., Wang, R., Huang, X.: Research and improvement of oscillation problems caused by active rectifier circuits in EV-WPT systems. IEEE Trans. Power Electron. 38(10), 13231–13242 (2023)
24. Deng, Z., Hu, H., Su, Y., Chen, F., Xiao, J., Tang, C., et al.: Design of a 60-kW EV dynamic wireless power transfer system with dual transmitters and dual receivers. IEEE J. Emerging Sel. Top. Power Electron. 12(1), 316–327 (2024)
25. Zhou, S., Chris Mi, C.: Multi-paralleled LCC reactive power compensation networks and their tuning method for electric vehicle dynamic wireless charging. IEEE Trans. Ind. Electron. 63(10), 6546–6556 (2016)
26. Xiang, L., Li, X., Tian, J., Tian, Y.: A crossed DD geometry and its double-coil excitation method for electric vehicle dynamic wireless charging systems. IEEE Access 6, 45120–45128 (2018)
27. Zaheer, A., Neath, M., Beh, H.Z.Z., Covic, G.A.: A dynamic EV charging system for slow moving traffic applications. IEEE Trans. Transp. Electrif. 3(2), 354–369 (2017)
28. Li, Y., Hu, J., Lin, T., Li, X., Chen, F., He, Z., et al.: A new coil structure and its optimization design with constant output voltage and constant output current for electric vehicle dynamic wireless charging. IEEE Trans. Ind. Inf. 15(9), 5244–5256 (2019)
29. Liu, Y., Mai, R., Liu, D., Li, Y., He, Z.: Efficiency optimization for wireless dynamic charging system with overlapped DD coil arrays. IEEE Trans. Power Electron. 33(4), 2832–2846 (2018)
30. Kamineni, A., Neath, M.J., Zaheer, A., Covic, G.A., Boys, J.T.: Interoperable EV detection for dynamic wireless charging with existing hardware and free resonance. IEEE Trans. Transp. Electrif. 3(2), 370–379 (2017)
31. Nagendra, G.R., Covic, G.A., Boys, J.T.: Sizing of inductive power pads for dynamic charging of EVs on IPT highways. IEEE Trans. Transp. Electrif. 3(2), 405–417 (2017)
32. Song, B., Cui, S., Dong, S., Zhang, M., Sun, T.: A systematic design methodology for the receiver structure in EV dynamic wireless charging system. IEEE Trans. Transp. Electrif. (2024). https://doi.org/10.1109/TTE.2024.3358633
33. Zhu, C., He, X., Yang, H., Luo, Y., Yang, B., Gao, J., et al.: A magnetic field concentration enhanced I-shaped transmitter for DWPT system to achieve low power fluctuation. IEEE Trans. Power Electron. 39(1), 1690–1700 (2024)
34. Triviño, A., Sánchez, J., Delgado, A.: Efficient methodology of the coil design for a dynamic wireless charger. IEEE Access 10, 83368–83378 (2022)
35. Sallan, J., Villa, J.L., Llombart, A., Sanz, J.F.: Optimal design of ICPT systems applied to electric vehicle battery charge. IEEE Trans. Ind. Electron. 56(6), 2140–2149 (2009)
36. Wang, S., Chen, J., Hu, Z., Rong, C., Liu, M.: Optimisation design for series–series dynamic WPT system maintaining stable transfer power. IET Power Electron. 10(9), 987–995 (2017)
37. Rakhymbay, A., Khamitov, A., Bagheri, M., Alimkhanuly, B., Lu, M., Phung, T.: Precise analysis on mutual inductance variation in dynamic wireless charging of electric vehicle. Energies 11(3), 624 (2018)

38. Zhang, Z., Pang, H., Lee, C.H.T., Xu, X., Wei, X., Wang, J.: Comparative analysis and optimization of dynamic charging coils for roadway-powered electric vehicles. IEEE Trans. Magn. 53(11), 1–6 (2017)
39. Liu, X., Clare, L., Yuan, X., Wang, C., Liu, J.: A design method for making an LCC compensation two-coil wireless power transfer system more energy efficient than an SS counterpart. Energies 10(9), 1346 (2017)
40. Triviño Cabrera, A., González González, J.M., Aguado, J.A.: Design and implementation of a cost-effective wireless charger for an electric bicycle. IEEE Access 9, 85277–85288 (2021)

How to cite this article: Quirós, J.C., Calvo, Á.L., Triviño, A., Guerrrero, E.V.: Time-domain design for misalignment-tolerant dynamic wireless charging. IET Power Electron. 18, e12777 (2025). https://doi.org/10.1049/pel2.12777